

# Calibration-free wavelength modulation for gas sensing in tunable diode laser absorption spectroscopy

L. J. Lan · Y. J. Ding · Z. M. Peng ·  
Y. J. Du · Y. F. Liu

Received: 21 June 2014 / Accepted: 8 October 2014 / Published online: 17 October 2014  
© Springer-Verlag Berlin Heidelberg 2014

**Abstract** A method is proposed that employs the ratios of the 2nd and 4th harmonics at the line center to measure line width under high absorption. The measured line width is then applied in the “calibration-free  $2f/1f$ ” formula to detect gas pressure and concentration. To verify this method, the transitions of CO<sub>2</sub> at 6,982.0678 cm<sup>-1</sup> and H<sub>2</sub>O at 6,979.2995 cm<sup>-1</sup> are selected to measure the line width, gas pressure, and concentration in laboratory and field environments, respectively. Experimental results are very consistent with the expectations.

## 1 Introduction

Tunable diode laser absorption spectroscopy (TDLAS) is widely used in gas detection because of its properties such as non-contact, speed, and high sensitivity [1–3]. Line shape is a critical factor in TDLAS because it possesses a finite line width that is caused by its various broadening mechanisms. In most cases, Doppler and collision are its most dominant forms of broadening mechanism (as described by Gaussian and Lorentzian profiles, respectively). Thus, line shape is the convolution of two profiles, namely the Voigt profile [4, 5], which can be described by the half widths at half maximum (HWHM, defined as line width) of the Lorentzian (collision broadening, determined from gas pressure, species concentration, and inherent characteristics of the line) and the Gaussian profiles (Doppler broadening, determined from gas temperature).

The advantage of direct absorption spectroscopy (DAS) is that it can directly determine both line widths and absorbance; thus, it can infer gas pressure, concentration, and temperature. However, DAS also has many disadvantages that have been proven by numerous researches [6–8]. Wavelength modulation spectroscopy (WMS) has high sensitivity and signal-to-noise ratio (SNR) to determine the gas parameters [9–13]. In WMS, line width is necessary to calculate the harmonics whether you use the 2nd harmonic detection or the “calibration-free  $2f/1f$ ” method [14–17]. As mentioned above, line widths are also determined by gas parameters. Scientists often use the gas temperature, pressure, species concentration, and spectroscopy constants in calculating the line widths to finally obtain the harmonic signals. In actual measurements, the uncertainty in gas parameters and spectroscopy constants will induce discrepancies between the simulated and experimental results.

The line widths in WMS have been receiving huge attention among researchers. However, many of the proposed methods [18–22] cannot effectively suppress the effect of laser intensity fluctuations because the laser should scan across the entire absorption feature. Hangauer et al. [23] put forward a method that reconstructed the laser transmission (used to infer the absolute line shape) by employing the harmonics at a single wavelength. This method can effectively eliminate the effect of laser intensity fluctuation. Nonetheless, a large modulation depth and higher harmonics should be used in measurements. For instance, the optimum number of harmonics is 20 when the modulation index is set to 3.0. In actual measurements, the SNR of higher harmonics is too low. Moreover, to detect the higher harmonics, the bandwidth of the detection system should be sufficiently high. Silver et al. [24] proposed a method that uses multiple harmonics to detect the absorption line shape. This invention employed the ratios

L. J. Lan · Y. J. Ding · Z. M. Peng (✉) · Y. J. Du · Y. F. Liu  
State Key Laboratory of Power Systems, Department of Thermal  
Engineering, Tsinghua University, Beijing 100084, China  
e-mail: apspect@mail.tsinghua.edu.cn

of various even harmonics at the line center to determine the Lorentzian broadening. This method is useful under low absorption (<5 %). However, the ratios would change if the absorbance increases, which leads to an erroneous measurement of line width. Meanwhile, as noted in the Figs. 4 and 5 in Ref. [24], the amplitudes of the high even harmonics (e.g., 4th, 6th, and 8th) sharply decreased. Thus, large modulation depths (modulation index ( $m$ ) is more than 10) were used to improve the SNR. Nevertheless, such over-modulation enhances the background signals, which has adverse effects on the measurement results [25–27].

Recently, we have proposed a method that utilized the ratios of the 2nd and 4th harmonics at the line center to measure line shape under low absorption conditions [28]. To address the aforementioned problems, this study employs the ratios of the 2nd and 4th harmonics at the line center to measure line width under high absorbance. Subsequently, the measured line width is utilized in the “calibration-free  $2f/1f$ ” formula that uses the 1st harmonic (with absorption, rather than its background) to normalize the 2nd harmonic for gas sensing. To assess the proposed method, the transitions of  $\text{CO}_2$  at  $6,982.0678 \text{ cm}^{-1}$  and  $\text{H}_2\text{O}$  at  $6,979.2995 \text{ cm}^{-1}$  are selected to detect line width, gas pressure, and concentration in laboratory and industrial fields, respectively.

## 2 Theory

### 2.1 “Calibration-free $2f/1f$ ” method under high absorption conditions

In Ref. [29], the background of the 1st harmonic was normalized with the 2nd harmonic. However, the background signals cannot be detected together with the absorption signals in real-time sensing, because the no-gas and gas absorption signals cannot be detected synchronously. The ratios of the 2nd and 1st harmonics of the absorption signals are given as follows [30]:

$$R_{21} = \frac{S_{2f}}{S_{1f}} = \frac{2 \int_{-\pi}^{\pi} \exp[-\alpha(v_0 + a \cos \theta)] \cos 2\theta \cdot d\theta}{i_0 \cos \psi_1 \int_{-\pi}^{\pi} \exp[-\alpha(v_0 + a \cos \theta)] \cdot (1 + \cos 2\theta) \cdot d\theta} \tag{1}$$

where  $S_{2f}$  and  $S_{1f}$  are the 2nd and 1st harmonics at the line center, respectively;  $i_0$  is the amplitude of the linear laser intensity modulation;  $\psi_1$  is the phase shift between the intensity and frequency modulation;  $i_0$  and  $\psi_1$  are the characteristic parameters of the diode laser;  $\alpha(v)$  is the spectral absorbance,  $\alpha(v) = PXS(T)L\varphi(v)$ , where  $P$  (atm),  $X$ ,  $S(T)$  ( $\text{cm}^{-2}/\text{atm}$ ), and  $L$  (cm) are the total gas pressure, volume concentration, line strength, and absorbing path length, respectively;  $v_0$  is the line center of the transition;

$a$  is the modulation depth;  $\varphi(v)$  ( $\text{cm}^{-1}$ ) is the line shape and written as:

$$\varphi(v) = \frac{\sqrt{\ln 2} \gamma_L}{\pi^{3/2} \gamma_G} \int_{-\infty}^{+\infty} \frac{\exp[-\ln 2 \cdot (t - v_0)^2 / \gamma_G^2]}{\gamma_L^2 + (v - t)^2} dt \tag{2}$$

where  $\gamma_L$  and  $\gamma_G$  are the line widths of the Lorentzian and Gaussian profiles, respectively. Olivero et al. [31] developed an empirical expression to calculate the line width of the Voigt profile, namely  $\gamma$ , and the modulation index is defined as:  $m = a/\gamma$ . These three line widths are given in Eq. (3), where  $M$  (g/mol) is the molecular weight of the absorbing species;  $\chi_{\text{self}}$  and  $\chi_{\text{air}}$  are the coefficients of self and air collisional broadening, respectively.

$$\begin{cases} \gamma = 0.5346\gamma_L + \sqrt{0.2166\gamma_L^2 + \gamma_G^2} \\ \gamma_L = P[X\chi_{\text{self}} + (1 - X)\chi_{\text{air}}] \\ \gamma_G = 3.581 \times 10^{-7} v_0 \sqrt{T/M} \end{cases} \tag{3}$$

Following our recent work [29] and Eq. (1), a new “calibration-free  $2f/1f$ ” formula that uses the 1st harmonic (with absorption) to normalize the 2nd harmonic to calculate the gas partial pressure is derived as follows: when the absorbance is less than 30 %,

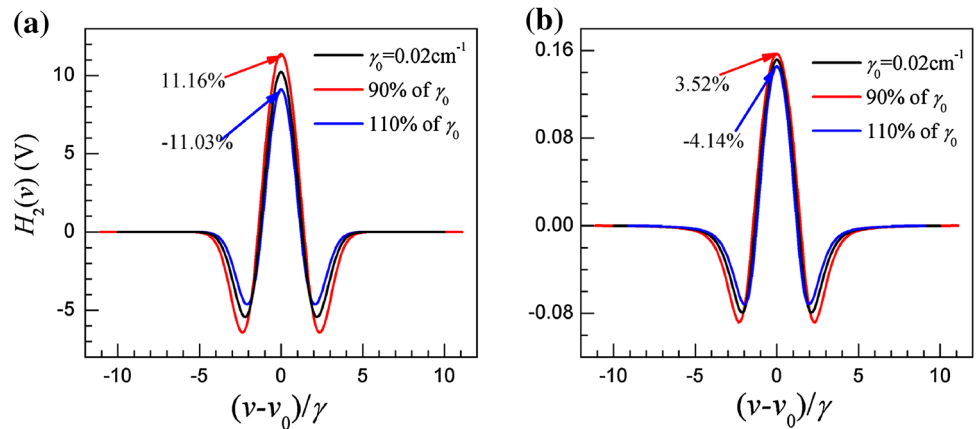
$$P_i = \frac{H_2 - Z(H_0 + \frac{H_2}{2}) + \sqrt{[H_2 - Z(H_0 + \frac{H_2}{2})]^2 + 2Z[T_2 - Z(T_0 + \frac{T_2}{2})]}}{S(T)L[T_2 - Z(T_0 + \frac{T_2}{2})]} \tag{4}$$

where  $Z = i_0 R_{21} \cos \psi_1$ ;  $P_i$  is the partial pressure,  $P_i = PX$ ;  $H_k$  is the  $k$ -th Fourier component of the line shape at the line center; and  $T_k$  is expressed by  $H_k$ .  $H_k$  and  $T_k$  can be computed using Eq. (5), where  $\delta_{k0}$  is the Kronecker delta. This delta is interpreted as 1 if  $k = 0$  and 0 if otherwise:

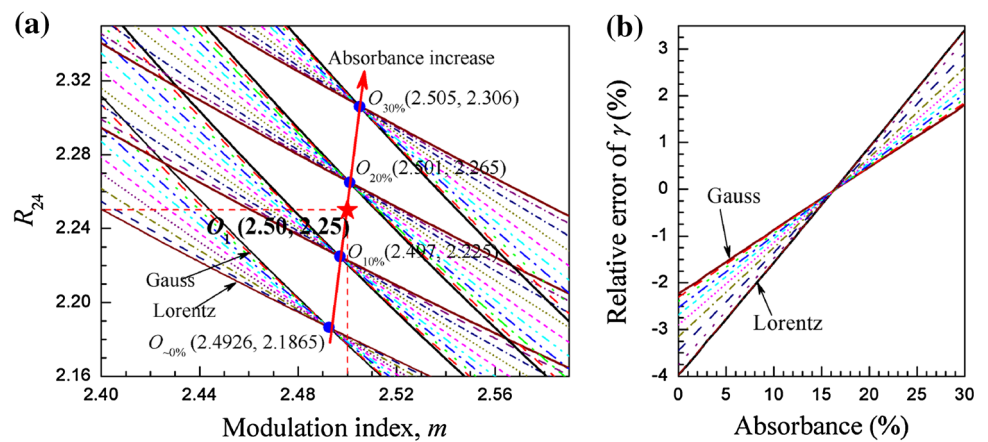
$$\begin{cases} H_k = \frac{1}{(1 + \delta_{k0})\pi} \int_{-\pi}^{\pi} \varphi(v_0 + a \cos \theta) \cos k\theta \cdot d\theta, \quad k = 0, 1, 2, \dots \\ T_0 = H_0^2 + \frac{1}{2}(H_1^2 + H_2^2 + H_3^2 + H_4^2 + \dots + H_k^2) \\ T_2 = \frac{1}{2}H_1^2 + 2H_0H_2 + H_1H_3 + H_2H_4 + H_3H_5 + \dots + H_kH_{k+2} \end{cases} \tag{5}$$

Figure 1 exhibits the influence of  $\pm 10\%$  line width uncertainties on  $H_2$  in the Gaussian and Lorentzian profiles, where the original line width is assumed to be  $0.02 \text{ cm}^{-1}$ . The line width of the Gaussian profile is more sensitive to the peak value than that of the Lorentzian profile; it is proven by the maximum relative error of 4.14 % obtained by the Lorentzian profile compared with the 11.16 % achieved by the Gaussian profile. Hence, the precision of line width is highly significant in improving the accuracy of real-time gas sensing especially in high-temperature or low-pressure

**Fig. 1** Influences on  $H_2$  when line width has  $\pm 10\%$  uncertainties with Gaussian and Lorentzian profiles ( $\gamma_0 = 0.02 \text{ cm}^{-1}$ ,  $a = 2.2\gamma_0$ ), **a** Gaussian profile, **b** Lorentzian profile



**Fig. 2 a** Ratios of  $S_{2f}$  and  $S_{4f}$  versus  $m$  at different absorbance (absorbance range is from 0 to 30 %); **b** relative errors of line width measurement versus absorbance with different line profiles when employing the approximate point  $O_1$



environments where Doppler broadening is prior to collision broadening.

### 2.2 Theory of measuring line width

According to the measuring techniques of WMS, when the influence of the nonlinear residual amplitude modulation (RAM) is ignored, the ratios of the 2nd and 4th harmonics at the line center can be written as follows:

$$R_{24} = \frac{S_{2f}}{S_{4f}} = - \frac{\int_{-\pi}^{\pi} \exp[-\alpha(v_0 + a \cos \theta)] \cdot \cos 2\theta \cdot d\theta}{\int_{-\pi}^{\pi} \exp[-\alpha(v_0 + a \cos \theta)] \cdot \cos 4\theta \cdot d\theta} \quad (6)$$

where  $S_{4f}$  is the 4th harmonics at the line center. Figure 2a depicts the numerical simulation results of  $R_{24}$  when the absorbance is less than 30 % by using Eq. (6) with different line profiles (the ratios of Lorentzian and Gaussian line widths) and modulation indices. At a specific absorbance, the values of  $R_{24}$  monotonously decrease and intersect at a fixed point with increasing modulation indices regardless of the variation in the line profiles. The fixed

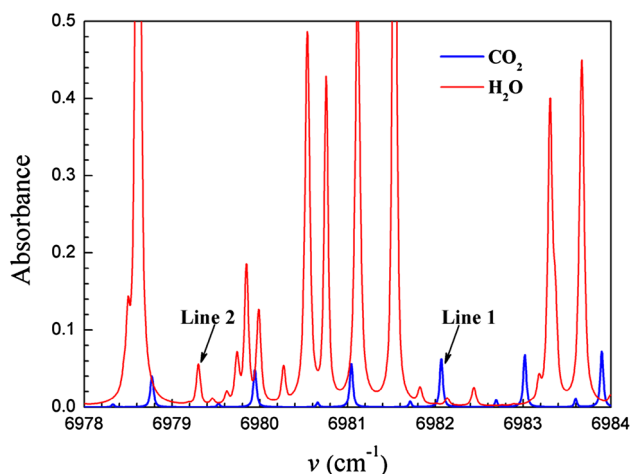
point changes with different absorbance. The horizontal and vertical coordinates of those fixed points both increase with absorbance. These coordinates can be calculated using Eq. (7), where  $\alpha(v_0)$  (below 30 %) is the absorbance at the line center.

$$\begin{cases} m^* = 2.4936 + 0.0331\alpha(v_0) + 0.01642\alpha(v_0)^2 \\ R_{24}^* = 2.1851 + 0.3949\alpha(v_0) + 0.02661\alpha(v_0)^2 \end{cases} \quad (7)$$

Based on these features, the line width of Voigt profile can be measured as follows: by changing the modulation depth, when  $R_{24} = R_{24}^*$ , there must be  $m = m^*$  regardless of the line profiles; thus, the line width can be calculated by  $\gamma = a^*/m^*$ , where  $a^*$  is the modulation depth. In practical applications, however, the exact values of absorbance are often unpredictable. Hence, an approximate point  $O_1(2.50, 2.25)$  is employed to estimate line width. Figure 2b reveals the measurement errors of line width given different absorbance and line profiles when this approximate point is applied. The errors range from  $-4.0$  to  $3.4\%$  when the absorbance is less than 30 %. Notwithstanding the errors induced by the use of the approximated fixed point, an

**Table 1** Spectroscopic constants for the selected transitions of CO<sub>2</sub> and H<sub>2</sub>O near 6,980 cm<sup>-1</sup>

	Molecular	$\nu_0$ (cm <sup>-1</sup> )	$T$ (K)	$S(T)$ (cm <sup>-2</sup> /atm)	$\chi_{\text{air}}$ (cm <sup>-1</sup> /atm)	$\chi_{\text{self}}$ (cm <sup>-1</sup> /atm)
Line 1	CO <sub>2</sub>	6,982.0678	293	$1.528 \times 10^{-3}$	0.0776	0.103
			650	$2.281 \times 10^{-4}$	0.0457	
Line 2	H <sub>2</sub> O	6,979.2995	293	$3.761 \times 10^{-5}$	0.0415	0.275
			650	$4.514 \times 10^{-4}$	0.0402	

**Fig. 3** Absorbance of CO<sub>2</sub> and H<sub>2</sub>O near 6,980 cm<sup>-1</sup> ( $T = 650$  K)

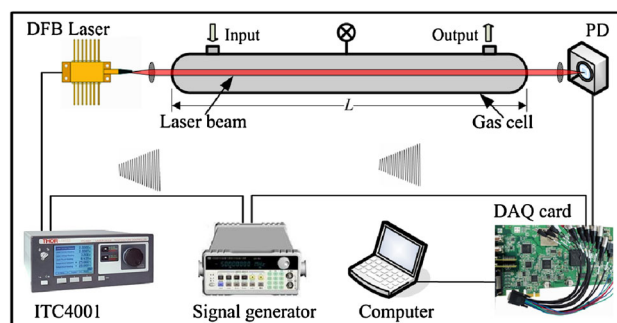
iterative algorithm can be adopted to improve the measurement precision, which is introduced in Sect. 3.

Given gas temperature and the measured line width, the Doppler and collision broadenings, the line shape and its Fourier components, the partial pressure can be gradually obtained according to Eqs. (2–5). The total gas pressure and concentration can finally be determined using the expressions of collision broadening and partial pressure. These measurement processes are discussed in the following section.

### 3 Verification experiments

The transitions of CO<sub>2</sub> and H<sub>2</sub>O near 6,980 cm<sup>-1</sup> are selected for our experiments to validate the proposed method. The spectroscopic constants of the selected transitions are acquired from the HITRAN 2008 database (Table 1).

In fact, the water content, such as the gas flue shown in Sect. 3.2, needs to be obtained in particular industrial applications. However, precisely matching the vapor concentration is difficult because the vapor easily coagulates at room temperature. To verify the accuracy of this proposed method, CO<sub>2</sub> (Line 1) is utilized to measure its pressure and concentration in laboratory

**Fig. 4** Experimental setup used to measure gas pressure and concentration in laboratory conditions

conditions. Figure 3 indicates the reason for line selection in the field measurements. For simulation, the gas temperature, total pressure, absorbing path length, CO<sub>2</sub>, and H<sub>2</sub>O concentration in the gas cell are assumed to be 650 K, 30.0 kPa, 360 cm, 15.0, and 8.0 %, respectively, while ignoring the absorptions of other gases. The absorbance of CO<sub>2</sub> and H<sub>2</sub>O is denoted by blue and red lines, respectively. Only Line 2 is suitable for the water content measurement in field detections because it is isolated from all the other lines and its absorbance is suitable for the technique.

#### 3.1 Laboratory experiments

The diagram of the experimental setup in the laboratory is shown in Fig. 4. The gas cell is filled with a CO<sub>2</sub>/N<sub>2</sub> mixture controlled by two mass flow controllers. A distributed feedback diode laser (NEL NLK1S5EAAA) with a center wavelength of 6,980 cm<sup>-1</sup> is employed as the spectroscopic source. The laser frequency is controlled by a diode laser controller (ITC4001). The light from the fiber-coupled diode laser is transmitted to a fiber collimator (Thorlabs F240APC-1550) and then sent through the gas cell. The optical power emitted from the gas cell is detected using a large-surface Ge photodiode (PDA50B-EC). The detected signals are recorded in a high-speed memory data acquisition (DAQ, the sampling rate is 320 kHz) card and modulated using a digital lock-in software (LabVIEW). Prior to tests, the laser is tuned to the line center by using a free space near infrared

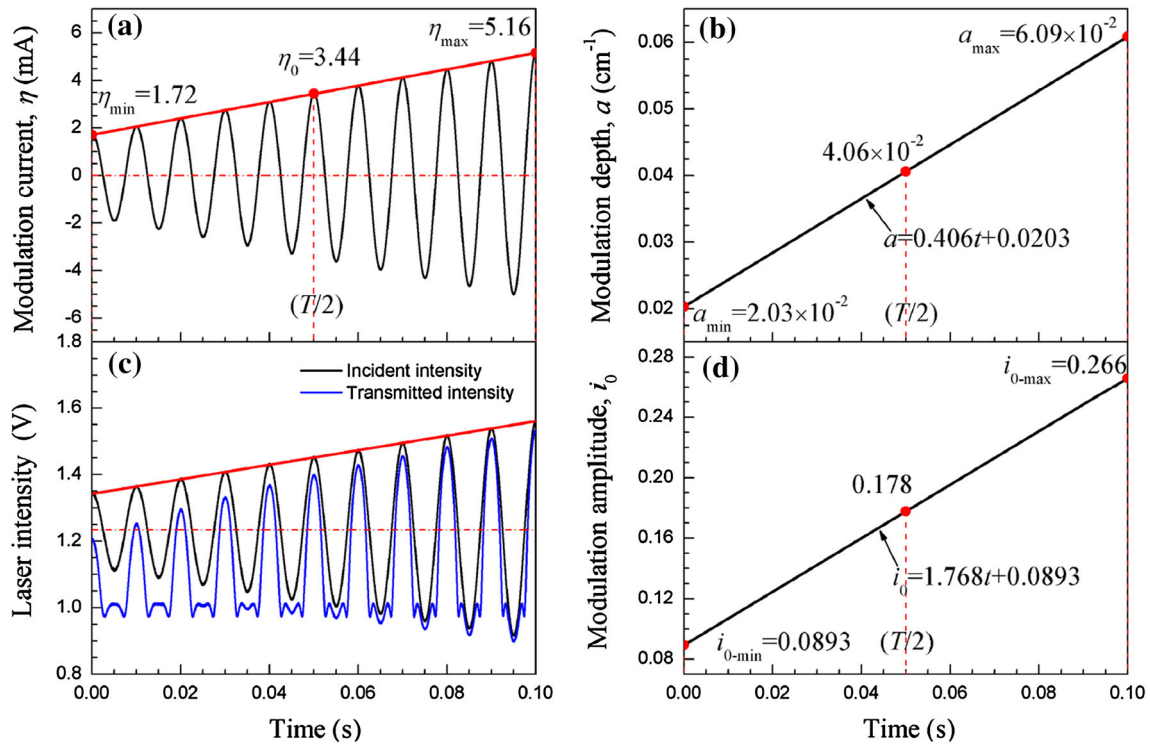


**Fig. 5** **a** Modulation current in a cycle, where the modulation frequency is reduced to 100 Hz to clearly show the signals; **b** modulation depth; **c** laser incident (no absorption) and transmitted

(with absorption) intensities; **d** modulation amplitude, which is determined using the laser incident intensity (no absorption)

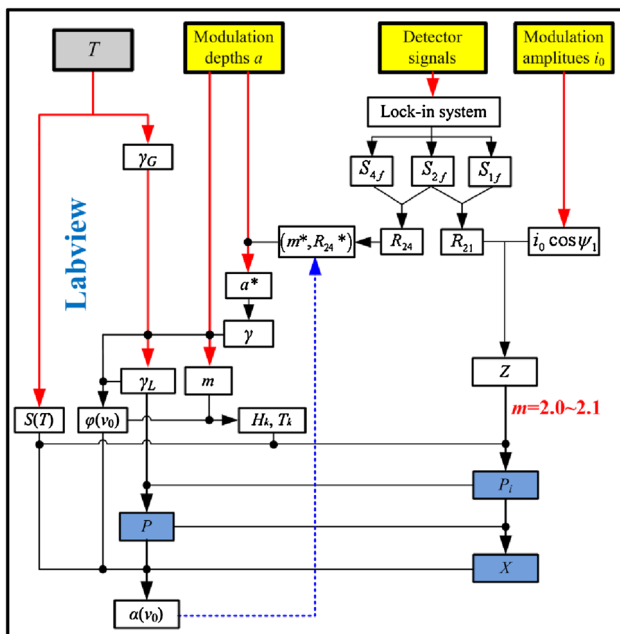


**Fig. 6** Calculation processes to measure gas pressure and concentration, where the modulation depths,  $a$ , and amplitudes,  $i_0$ , are corresponding to each other

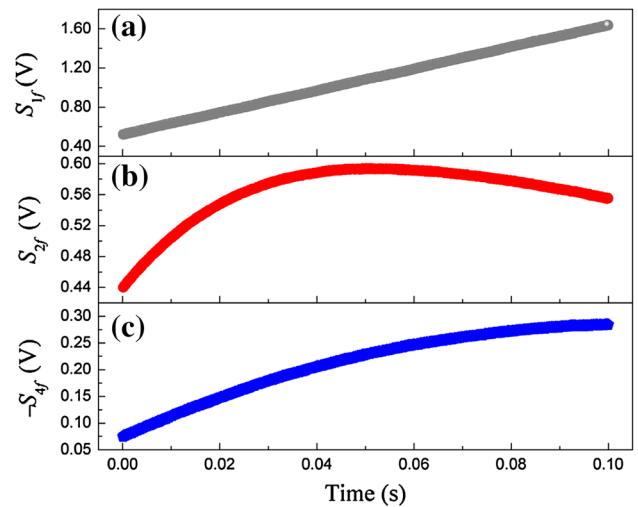


**Fig. 7**  $S_{1f}$ ,  $S_{2f}$ , and  $S_{4f}$  at the line center recorded by lock-in software in an amplitude modulation cycle, which are the means of 10 sequential scans

wavelength meter (Bristol 621B). An external high-frequency sinusoidal modulation signal created by a signal generator is added to the diode laser controller to produce harmonics.

In laboratory conditions, the current and the temperature of the diode laser are set to 27.9 mA and 19.866 °C, respectively, to stabilize the laser frequency at the line center (6,982.0678 cm<sup>-1</sup>), where the current tuning rate (changes in laser frequency with variations of 1 mA) and phase shift  $\psi_1$  are approximately  $1.18 \times 10^{-2}$  cm<sup>-1</sup>/mA and 36° when the modulation frequency signal is 2.5 kHz. The modulation signal is an amplitude linear varying sine signal, as shown in Fig. 5a. The formula is given as:

$$\eta(t) = \left[ \eta_0(1 - x) + \frac{2\eta_0x}{T}t \right] \cos(2\pi ft), \quad 0 \leq t < T \quad (8)$$

where  $\eta(t)$  (mA) is the current of sinusoidal modulation;  $\eta_0$  is the modulation current at  $T/2$ ;  $T$  (s) is the amplitude-varying cycle (low frequency);  $x$  is the modulation level,  $x \in [0, 1]$ ;  $f$  (Hz) is the sinusoidal modulation frequency (high frequency).

The calculation processes are exhibited in Fig. 6. Figures 7 and 8 display a typical example of the measurement processes in one experiment where gas temperature, absorbing path length, the partial, and the total pressures are  $296.0 \pm 0.2$  K, 120 cm,  $7.50 \pm 0.20$  kPa, and  $19.75 \pm 0.10$  kPa, respectively.  $\eta_0$ ,  $x$ ,  $T$ , and  $f$  are 3.44 mA, 0.5, 0.1 s, and 2.5 kHz, respectively.

When the modulation depths and amplitudes are determined, the line width and the gas parameters can be measured through the following processes: first, the signals from the detector are entered into LabVIEW through a DAQ card. The 1st, 2nd, and 4th harmonics at the line center with every modulation depths are demodulated using the lock-in software. The three measured harmonics,

which are represented by the average of 10 sequential scans to improve SNR, are shown in Fig. 7.

The values of  $R_{24}$  and  $Z$  versus modulation depths which are acquired through the relationships between the time and the modulation depth are shown in Fig. 8a, b, respectively. As mentioned in Sect. 2.2, the line width can be calculated using the approximate fixed point ( $\gamma = a^*/m^*$ ), where  $a^*$  ( $4.860 \times 10^{-2}$  cm<sup>-1</sup>) is the modulation depth corresponding to  $R_{24}^* = 2.25$ . Therefore, the line width is computed ( $1.944 \times 10^{-2}$  cm<sup>-1</sup>). The modulation indices within the modulation cycle are generated (displayed at the bottom of Fig. 8a) from dividing the measured line width by modulation depths. By substituting the measured line width and Doppler broadening ( $\gamma_G = 6.441 \times 10^{-3}$  cm<sup>-1</sup>) into Eq. (3), the collision broadening is then estimated ( $\gamma_L = 1.717 \times 10^{-2}$  cm<sup>-1</sup>). Consequently, the line shape is obtained.

Figure 8b presents the values of  $Z = i_0R_{21}\cos\psi_1$  with different modulation indices. As indicated in Eq. (4), the proposed method uses  $Z$  at a certain modulation index ( $m = 2.0-2.1$ ) to calculate the partial pressure. For instance, when  $m = 2.05$ ,  $P_i = 7.68$  kPa where the values of  $Z$ ,  $H_0$ ,  $H_2$ ,  $T_0$ , and  $T_2$  are 0.0779, 7.370,  $-6.077$ , 75.899, and  $-1.060$ , respectively. All of the results are then averaged (7.67 kPa). Subsequently, the total pressure and volume concentration can be obtained as 19.95 kPa and 38.50 %, respectively.

Finally, since the use of the approximate fixed point (2.50, 2.25) in measuring the line width generates certain measurement errors, an iterative algorithm (the dotted blue line exhibited in Fig. 6) is adopted to limit the deviations in

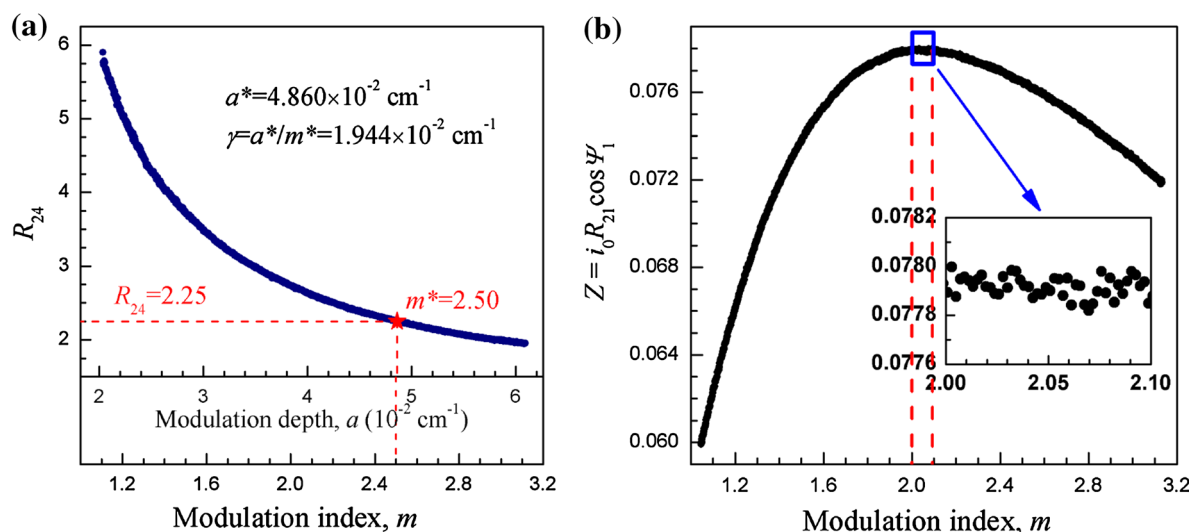


**Fig. 8 a** Ratios of  $S_{2f}$  and  $S_{4f}$  versus modulation depth and modulation index in an amplitude modulation cycle; **b** The curve of  $Z$  versus modulation index; the process employs the values of  $Z$  when

$m$  ranges from 2.0 to 2.1 to calculate partial pressure, which can improve the measurement precision

the detection. The absorbance at the line center  $\alpha(\nu_0)$  is estimated as 23.46 % by using Eq. (1). A new fixed point  $O_2$  ( $m_2^* = 2.502$ ,  $R_{24.2}^* = 2.279$ ) is then calculated through Eq. (7). Subsequently, the new modulation depth and line width are denoted as  $a_2^* = 4.823 \times 10^{-2} \text{ cm}^{-1}$  and  $\gamma_2 = a_2^*/m_2^* = 1.928 \times 10^{-2} \text{ cm}^{-1}$ , respectively. Similar to the calculation process above, the partial and total pressures,  $\text{CO}_2$  concentration, and absorbance are 7.60 kPa and 19.73 kPa, and 38.52, and 23.48 %, respectively. Obviously, the process does not need to be reiterated because the difference between the twice-measured absorbance is only 0.02 %.

The above detection period is extended to 12 min to investigate the reliability and accuracy of the proposed method at laboratory conditions. The means and standard

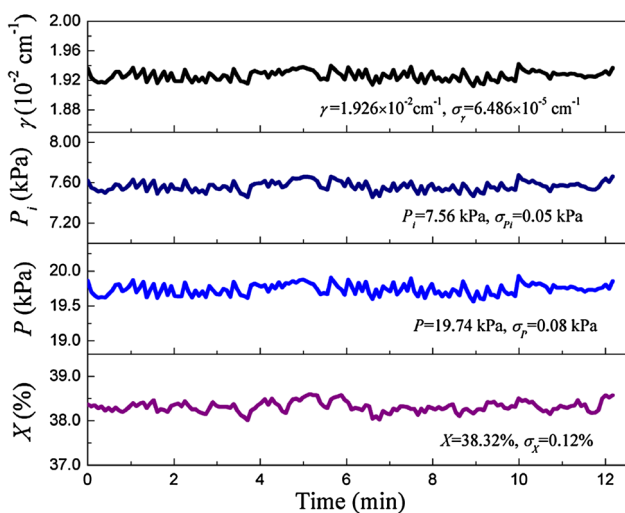


**Fig. 9** A long-time detection results of the line width,  $\text{CO}_2$  partial pressure, total pressure, and  $\text{CO}_2$  concentration obtained from the LabVIEW program ( $T = 296.0 \pm 0.2 \text{ K}$ ,  $L = 120 \text{ cm}$ ,  $P_i = 7.50 \pm 0.20 \text{ kPa}$ , and  $P = 19.75 \pm 0.10 \text{ kPa}$ )

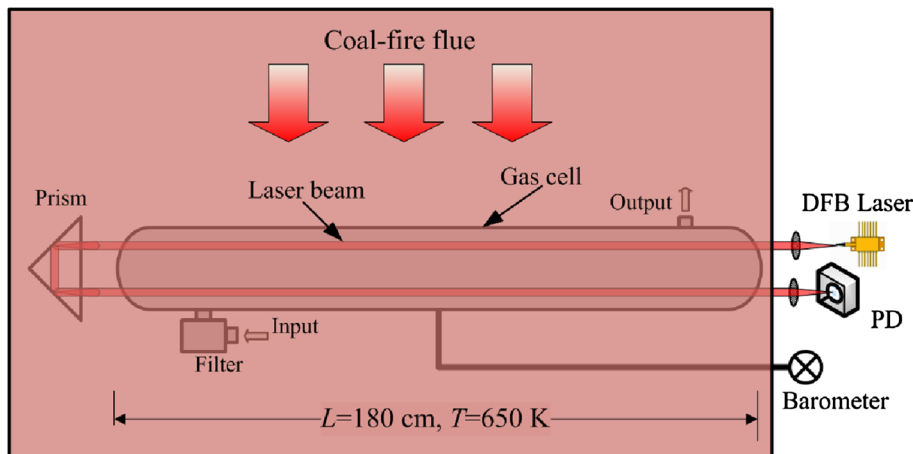
deviations ( $\sigma$ ) of line width,  $\text{CO}_2$  partial pressure, total pressure, and  $\text{CO}_2$  concentration are marked in Fig. 9. These findings indicate that the proposed method has high accuracy in measuring gas pressure and concentration at laboratory conditions.

### 3.2 Field measurements

The following are the concentration measurements of water vapor in a 300-MW industrial boiler unit located in a power plant. The concentration of particles in the chimney flue reaches  $50 \text{ g/Nm}^3$ , and such thick layer of particles is difficult for the laser to transmit through. Thus, the exhaust gases are pumped out using a vacuum pump, transported through a filter, and then transmitted into an isolated gas chamber to be measured, as shown in the schematic diagram in Fig. 10. The gas chamber is positioned between the SCR DeNOx reactor and the air preheater. It is then horizontally inserted into the flue and heated using the hot gas (about 650 K). The laser beam is reflected through a prism and then detected by the PD. The pressure is maintained by controlling the inlet and outlet valves and detected using a barometer. However, the barometer cannot work at high temperatures. Therefore, a long tube is used to transform the hot gas into a cold air, leading to deviations of the pressure measurement (within  $\pm 10 \%$ ).

Figure 11 exhibits the measurement results at full-load working condition (270 MW). The pressure in the gas cell is about 26 kPa ( $\pm 3 \text{ kPa}$ ). The current coal consumption and primary air are 100 and 230 t/h, respectively. Obviously, the measured total pressure (25.78 kPa) is approximately to the set value. Moreover, the concentration of water vapor (8.06 %) is in accordance with the design value at full-load working condition (about 8.0 %). Likewise, Fig. 12 shows the measurement results at half-load condition (approximately 130 MW), where the pressure is around 38 kPa ( $\pm 4 \text{ kPa}$ ). The vapor concentration at half-

**Fig. 10** Experimental setup used for gas sensing in the flue



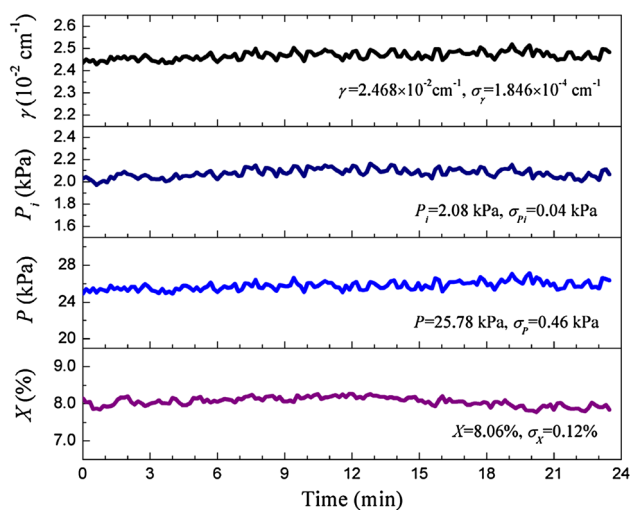


**Fig. 11** Experimental results under full-load working condition (270 MW) (The coal consumption and primary air are 100 and 230t/h, which indicates that the air fuel ratio is 2.30)

load condition is lower (about 6.0 %) than that at full-load because the water vapor in the exhaust gas mainly originates from the combust. The air fuel ratio at full-load (2.30) is lower than that at half-load condition (2.50). In sum, a large air fuel ratio indicates a low vapor concentration.

In Fig. 12, the coal consumption, primary air, and system load are initially set as 56 t/h, 140t/h, and 135 MW, respectively. To investigate the sensitivity of the proposed method in field measurements, 1 h later, the primary air is constant, whereas the coal consumption and load are reduced to 54/h and 128 MW, respectively (the air fuel ratio is 2.60). The measurements indicate the varied burning in the hearth. For example, the concentrations of water vapor decreases from 6.04 to 5.74 %. Moreover, the detected values sharply changed in only 4 min after the amount of coal decreased. Thus, the proposed method can measure the gas pressure and concentration in field environments with high precision and sensitivity.

#### 4 Conclusions

In this paper, a method is proposed to measure gas pressure and concentration. First, the ratios of the 2nd and 4th harmonics at the line center are used to measure line width. Then, the gas pressure and concentration are estimated using the measured line width and the “calibration-free  $2f/1f$ ” method. To verify this method, the transition of  $\text{CO}_2$  at  $6,982.0678 \text{ cm}^{-1}$  is selected to measure gas pressure and concentration in laboratory conditions; and to extend its application, the transition of  $\text{H}_2\text{O}$  at  $6,979.2995 \text{ cm}^{-1}$  is used to measure vapor concentration in industrial fields.

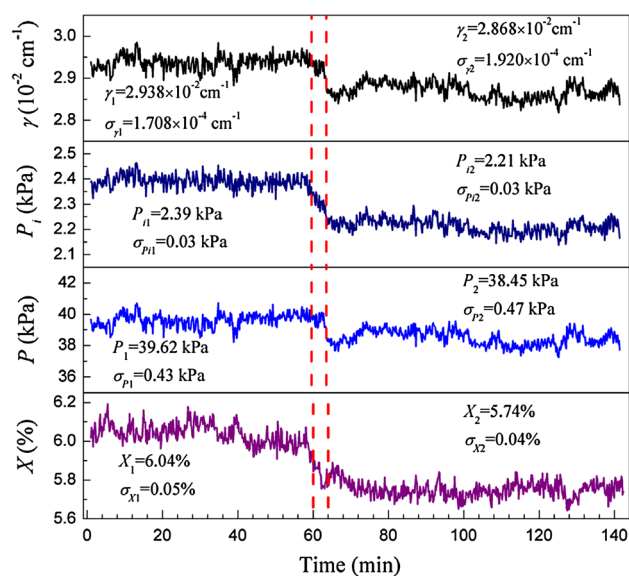


**Fig. 12** Experimental results under half-load working condition. (At the first hour, the air fuel ratio is 2.50; 1 h later, the air fuel ratio is changed to be 2.60)

The experimental results coincide well with the expectations and indicate that this technique has high precision and sensitivity in gas sensing. The proposed method employs the low (1st, 2nd, and 4th) harmonics at the line center to calculate gas parameters; thus, it contains the advantages of WMS (e.g., high SNR and sensitivity). As such, it can effectively eliminate the effects of laser intensity fluctuations. Most importantly, this method uses the measured line width rather than the calculated one to determine the gas pressure and concentration. Therefore, it can easily account for any fluctuation in gas parameters, such as partial and total pressures, during real-time detection.

However, the proposed method is also practically limited. For instance, the absorption feature must either be completely isolated or the distance between adjacent lines must be more than five times than that of the line widths of the selected lines. Moreover, because the SNR of 4th harmonics is poor, the background signals cannot be ignored under weak absorption conditions. Hence, if background signals can be eliminated, the optimum peak absorbance range of this method is 0.1–30 %.

**Acknowledgments** This work was supported by the National Natural Science Foundation of China under Grant Nos. 51206086 and 51176085.

#### References

- O. Witzel, A. Klein, C. Meffert, S. Wagner, S. Kaiser, C. Schulz, V. Ebert, *Opt. Express* **21**, 19951 (2013)
- K. Sun, X. Chao, R. Sur, J.B. Jeffries, R.K. Hanson, *Appl. Phys. B* **110**, 497 (2013)



3. C.T. Zheng, W.L. Ye, J.Q. Huang, T.S. Cao, M. Lv, J.M. Dang, Y.D. Wang, *Sens. Actuators, B* **190**, 249 (2014)
4. Y.Y. Liu, J.L. Lin, G.M. Huang, Y.Q. Guo, C.X. Duan, *J. Opt. Soc. Am.* **18**, 666 (2001)
5. E. Detommasi, A. Castrillo, G. Casa, L. Gianfrani, *J. Quant. Spectrosc. Radiat. Transf.* **109**, 168 (2008)
6. S. Hunsmann, K. Wunderle, S. Wagner, U. Rascher, U. Schurr, V. Ebert, *Appl. Phys. B* **92**, 393 (2008)
7. Y.J. Ding, X.H. Li, Z.M. Peng, L. Che, *Spectrosc. Lett.* **46**, 465 (2013)
8. Z.M. Peng, Y.J. Ding, J.W. Jia, L.J. Lan, Y.J. Du, Z. Li, *Opt. Express* **21**, 23724 (2013)
9. J.T.C. Liu, J.B. Jeffries, R.K. Hanson, *Appl. Phys. B* **78**, 503 (2004)
10. J. Reid, D. Labrie, *Appl. Phys. B* **26**, 203 (1981)
11. L. Tao, K. Sun, M.A. Khan, D.J. Miller, M.A. Zondlo, *Opt. Express* **20**, 28106 (2012)
12. P. Kluczynski, J. Gustafsson, A.M. Lindberg, O. Axner, *Spect. Acta B* **56**, 1277 (2001)
13. T.D. Cai, H. Jia, G.S. Wang, W.D. Chen, X.M. Gao, *Sens. Actuators A Phys.* **152**, 5 (2009)
14. T. Fernholz, H. Teichert, V. Ebert, *Appl. Phys. B* **75**, 229 (2002)
15. R.T. Wainner, B.D. Green, M.G. Allen, M.A. White, J. Stafford-Evans, R. Naper, *Appl. Phys. B* **75**, 249 (2002)
16. G.B. Rieker, J.B. Jeffries, R.K. Hanson, *Appl. Opt.* **48**, 5546 (2009)
17. L. Che, Y.J. Ding, Z.M. Peng, X.H. Li, *Chin. Phys. B* **21**, 127803 (2012)
18. J. Henningsen, H. Simonsen, *Appl. Phys. B* **70**, 627 (2000)
19. K. Duffin, A.J. McGettrick, W. Johnstone, G. Stewart, D.G. Moodie, *J. Lightwave Technol.* **25**, 3114 (2007)
20. G. Stewart, W. Johnstone, J.R.P. Bain, K. Ruxton, K. Duffin, *J. Lightwave Technol.* **29**, 811 (2011)
21. L. Li, N. Arsad, G. Stewart, G. Thursby, B. Culshaw, Y.D. Wang, *Opt. Commun.* **284**, 312 (2011)
22. Z.M. Peng, Y.J. Ding, L. Che, Q.S. Yang, *Opt. Express* **20**, 11976 (2012)
23. A. Hangauer, J. Chen, R. Strzoda, M.-C. Amann, *Appl. Phys. B* **110**, 177 (2013)
24. J.A. Silver, D.S. Bomse, *Pat. US 6356350* (1999)
25. H. Li, G.B. Rieker, X. Liu, J.B. Jeffries, R.K. Hanson, *Appl. Opt.* **45**, 1052 (2006)
26. K. Ruxton, A.L. Chakraborty, W. Johnstone, M. Lengden, G. Stewart, K. Duffin, *Sens. Actuators, B* **150**, 367 (2010)
27. J. Gustafsson, N. Chekalin, O. Axner, *Spect. Acta B* **58**, 123 (2003)
28. L.J. Lan, Y.J. Ding, Z.M. Peng, Y.J. Du, Y.F. Liu, Z. Li, *Appl. Phys. B* **117**, 543 (2014)
29. Z.M. Peng, Y.J. Ding, L. Che, X.H. Li, K.J. Zheng, *Opt. Express* **19**, 23104 (2011)
30. A. Farooq, J.B. Jeffries, R.K. Hanson, *Appl. Phys. B* **96**, 161 (2009)
31. J.J. Olivero, R.L. Longbothum, *J. Quant. Spectrosc. Radiat. Transf.* **17**, 233 (1977)